1

Introduction

Cold collisionless fluid that explains many observations in astrophysics and cosmology. It's existence shouldn't be questioned, only its microphysical constitution.

1.1 Evidence for Dark Matter

Today, the amount of evidence in support of dark matter's existence is overwhelming. This evidence comes from astrophysical and cosmological observations that are inconsistent with a universe composed entirely of visible matter. This section serves as a review of this evidence.

1.1.1 Astrophysical Observations

Galaxy Clusters

Some of the first hints for the existence of dark matter came from observations of galaxy clusters. Perhaps the most famous analysis was performed by Fritz Zwicky [1], who was puzzled by the high rotational velocities of galaxies within the Coma Cluster. By applying the virial theorem, equating the cluster's kinetic and gravitational potential energies, he found that the cluster would need to contain a much more significant amount of *dunkle materie* (dark matter) than visible matter to accommodate these high velocities.

Rotation Curves of Spiral Galaxies

The anomalous rotational velocities observed in galaxy clusters can also be observed at the galactic scale. The rotation curves of spiral galaxies, which relate the rotational velocities of stars to their distance from the galactic centre, were observed to be flat at large distances. From the observed distribution of visible matter, Newtonian mechanics predicts that the orbital velocity of a star a distance r from the galactic centre, $v_\star(r)$, is related to the mass contained within a radius r, $M(r)$, through

$$v_\star(r) = \sqrt{\frac{GM(r)}{r}}, \tag{1.1}$$

indicating that the velocity should fall off as $1/\sqrt{r}$ at the outer regions of the galaxy where $M(r)$ is constant. Instead, observations of many spiral galaxies indicate that this velocity remains constant out to the galaxy's edge.

A simple way to produce such a rotation curve is to introduce a spherically symmetric distribution of dark matter surrounding the galaxy,

$$\rho_{\mathrm{DM}}(r) = \frac{v_0^2}{4\pi G r^2}, \tag{1.2}$$

which results in a constant rotational velocity of v_0 out to the galaxy edge. Detailed simulations of structure formation in a Cold Dark Matter (CDM) Universe indicate that the true distribution is better represented by distribution functions such as the Navaro-Frenk-White (NFW) profile [2, 3] or Einasto [4] profiles, which are commonly used in the literature.

An example rotation curve for galaxy NGC 6503 is presented in Fig. 1.1, with the contributions from each of the matter components to the rotational velocity shown [5, 6]. As can be seen, the visible matter constituting disk and gas components does not explain the observed rotational velocity.

Gravitational Lensing

As described by General Relativity, the curvature of space-time around massive entities causes light to travel along curved paths. As such, the mass of astrophysical structures can be deduced from the extent to which they distort the images of objects in the background. The extent of the distortions depends on how massive the foreground object is, ranging from the shearing of the background image (weak lensing), to multiple copies of the background object appearing (strong lensing) [7]. The disparity between the mass obtained from gravitational lensing and the mass of visible matter in the system is further evidence of dark matter's existence [8, 9].

Rotation Curve for NGC 6503
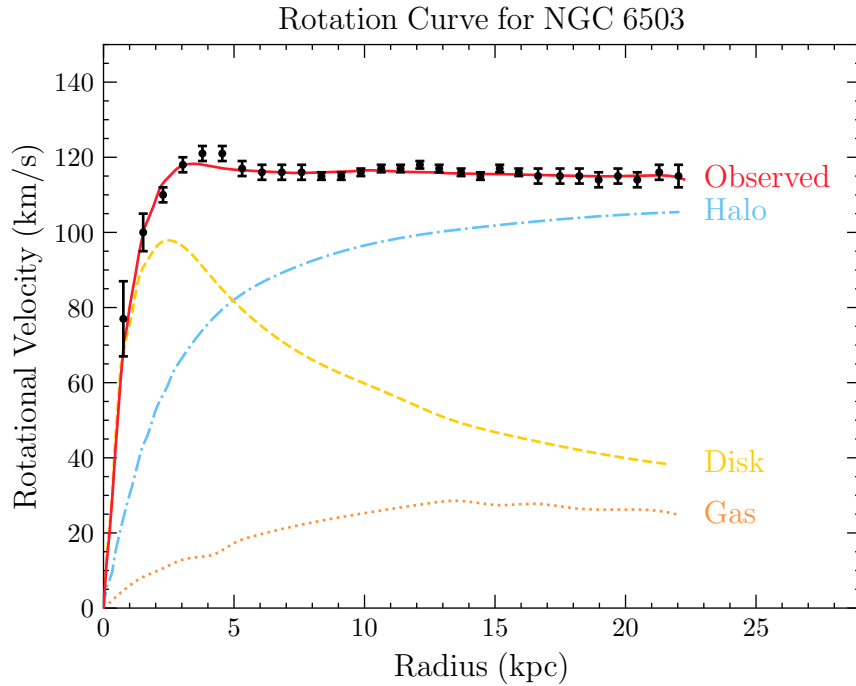
Figure 1.1: Galaxy rotation curve for NGC 6503, showing the contributions to the total velocity (red) from the DM halo (blue), disk (yellow), and gas components. Data used in making this plot was obtained from [5, 6].

The Bullet Cluster

The galaxy cluster 1E 0657-56, commonly referred to as the "bullet-cluster", was formed by the collision of two separate galaxy clusters. The baryonic matter in these clusters is mostly composed of a strongly interacting gas, and as expected produced a significant amount of X-rays during the collision. These X-rays were imaged by the Chandra X-Ray telescope [10], providing information on the resulting distribution of the visible matter. This is shown by the red regions of Fig. 1.2, where it can be seen how the visible matter has been smeared due to the collision. However, when the gravitational potential was mapped using gravitational lensing, it was clear that the majority of the mass was displaced relative to the visible matter. This mass is attributed to the dark matter components of the original clusters. As indicated by the purple regions in Fig. 1.2, the dark matter halos seem to have passed through each other mostly unperturbed. This tells us that not only is the majority of the mass comprised of dark matter, but that the dark matter has extremely weak interactions with both the visible matter and itself.

Figure 1.2: Image of the Bullet Cluster with contours of the gravitational potential superposed. The red regions indicate the baryonic matter after the collision, while the purple regions are the expected DM components deduced from gravitational lensing. [10, 11]

1.1.2   Cosmological Evidence

The current best cosmological model is the Λ-Cold Dark Matter model (ΛCDM), in which Λ refers to the cosmological constant associated with dark energy, and as the name suggests, cold (i.e. non-relativistic) dark matter plays a prominent role. The key components of this model are the aforementioned dark energy and dark matter, along with baryonic matter, and assumes that gravity is described by Einstein's General Relativity. The total energy density of the universe, $\rho_{\text{Univ.}}$, is broken down into three components based on how their density redshifts with the expansion of the Universe. In the ΛCDM model, these components are matter, radiation, and the vacuum energy Λ. The cosmological abundances of each component, (Ω_{m}, Ω_{r}, Ω_{Λ} respectively), are expressed as a fraction of the critical density, ρ_{crit},

$$\rho_{\text{crit}} = \frac{H^2}{8\pi G_N}, \tag{1.3}$$

$$\Omega_i = \frac{\rho_i}{\rho_{\text{crit}}}, \tag{1.4}$$

where H is the Hubble parameter, such that the total energy density of the Universe satisfies

$$\Omega_{\mathrm{m}} + \Omega_{\mathrm{r}} + \Omega_{\Lambda} = \frac{\rho_{\mathrm{Univ.}}}{\rho_{\mathrm{crit}}}. \tag{1.5}$$

The ratio $\rho_{\mathrm{Univ.}}/\rho_{\mathrm{crit}}$ determines the curvature of the universe, with values greater than 1 corresponding to a closed universe, less than 1 to an open universe, and equal to 1 to a spatially flat universe. Current observations are consistent with a spatially flat universe, and so we have $\sum_i \Omega_i = 1$.

The ΛCDM model has seen huge success as it provides explanations for observed the power spectrum of the Cosmic Microwave Background (CMB), the large-scale structure of the Universe, the abundances of light elements (hydrogen, deuterium, helium, and lithium), and the accelerated expansion rate of the Universe. These observations constrain the parameters of the model, and hence provide a complimentary probe of the properties of dark matter to the astronomical observations discussed above.

The Cosmic Microwave Background

One of the strongest probes of cosmological models is the Cosmic Microwave Background (CMB), relic photons from the time epoch of last scattering. This occurred after recombination, at a temperature of around $\sim 3000\,\mathrm{K}$, once the photons had decoupled from the baryonic matter and could freely propagate through the universe. The photons observed today have been redshifted by the expansion of the Universe, and are well described by a blackbody spectrum with a temperature of $T_{\mathrm{CMB}} = 2.73 \pm 0.0006\,\mathrm{K}$. Observations of the CMB temperature reveal that it is not exactly isotropic, with anisotropies at the level of $\delta T_{\mathrm{CMB}}/T_{\mathrm{CMB}} \sim 10^{-5} - 10^{-6}$ seen on a range of angular scales in the sky. These anisotropies were seeded by the primordial density perturbations that arise during inflation. These perturbations evolve due to the acoustic oscillations of the photon-baryon plasma driven by the interplay between the pressure from the photons and the gravitational attraction of the matter. The oscillations cease once the photons decouple, freezing in their temporal phases that are observed as peaks in the angular power spectrum of the temperature anisotropies.

Measurements of the CMB power spectrum provide information on many of the cosmological parameters. The locations of the acoustic peaks depend on the spatial geometry of the Universe and hence constrains Ω_{tot}. The total matter density, Ω_{m}, affects how the CMB spectrum is gravitationally lensed. The relative amplitudes of the peaks probe the baryon-to-photon ratio and hence the baryon density, Ω_{b}. Finally, the density of dark matter, Ω_{DM}, is obtained by fitting the cosmological parameters to the exact shape of the spectrum [5, 12].

The Planck collaboration most recently performed a precise measurement of the CMB power spectrum in 2018, obtaining best-fit parameters [12, 13]

$$\Omega_{\mathrm{m}} = 0.311 \pm 0.006, \quad \Omega_\Lambda = 0.689 \pm 0.006, \tag{1.6}$$

for the matter and dark energy densities. They obtained a total energy density of $\Omega_{\mathrm{tot}} = 1.011 \pm 0.006$ at 68% confidence level, providing strong evidence for a spatially flat Universe. The contributions to the matter density from the dark and baryonic components were found to be

$$\Omega_{\mathrm{DM}} h^2 = 0.1193 \pm 0.0009, \quad \Omega_{\mathrm{b}} h^2 = 0.02242 \pm 0.00014, \tag{1.7}$$

where h is the dimensionless Hubble constant such that the Hubble parameter today is $H_0 = 100\,h\,\mathrm{km\,s^{-1}}$ Mpc.

Large Scale Structure

After recombination, the pressure on the baryonic matter from photons began to decrease, eventually allowing the small density perturbations to grow. This led to the growth of stars, galaxies, and the large-scale structure we observe today [14]. N-body simulations of the Universe's evolution require a cold dark matter component for this structure to form. While a small component of the dark matter can be warm, hot dark matter would wash out small-scale structures [15].

1.2   Potential Models of Dark Matter

Given that baryonic matter is composed of particles described by the Standard Model (SM) of particle physics, it is a fair assumption that dark matter will also have a particle nature. Therefore, models of particle dark matter are built by extending the SM in a way consistent with its symmetries. Such models may be as simple as introducing a single new field into the SM, or there may be a more extensive hidden sector with a complicated symmetry structure. Additionally, there are compelling theories in which dark matter is not a fundamental particle, such as primordial black holes (PBHs) formed in the early universe. Given the few details we know about dark matter, there exists an enormous library of viable dark matter candidates. However, there are generic properties a good dark matter candidate must satisfy, namely:

- **Stable on Cosmological Timescales:** Dark matter must either be stable or have a lifetime significantly longer than the age of the Universe to be present in its current abundance.
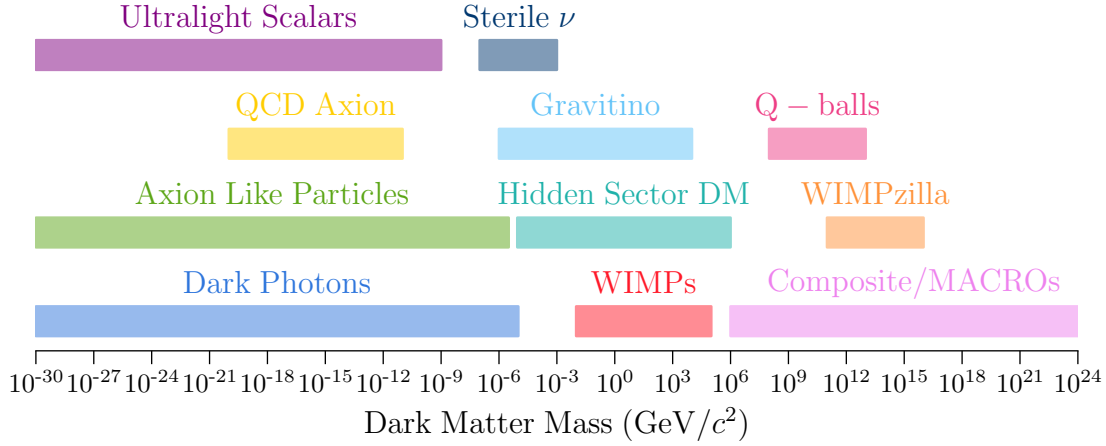
Figure 1.3: Illustrative landscape of dark matter models and the mass range for which they predict a valid candidate.

- **Neutral or milli-charged under Electromagnetism:** Dark matter, as its name suggests, does not significantly interact with light. Requiring that dark matter be completely decoupled from the Standard Model plasma by the time of recombination yields an upper bound on the electric charge the dark matter can carry of [16]

$$q_{\mathrm{DM}}/e < \begin{cases} 3.5 \times 10^{-7} \left(\frac{m_{\mathrm{DM}}}{1\,\mathrm{GeV}}\right)^{0.58}, & m_{\mathrm{DM}} > 1\,\mathrm{GeV} \\ 4.0 \times 10^{-7} \left(\frac{m_{\mathrm{DM}}}{1\,\mathrm{GeV}}\right)^{0.35}, & m_{\mathrm{DM}} < 1\,\mathrm{GeV} \end{cases} \tag{1.8}$$

- **Small Self-Interactions:** The standard ΛCDM cosmology assumes that the dark matter is collisionless. However, small dark matter self-interactions can help resolve existing small-scale structure issues [17, 18]. Current limits on the self-interaction cross-section are $\sigma_{\mathrm{DM-DM}}/m_{\mathrm{DM}} < 0.48\,\mathrm{cm}^2/\mathrm{g}$ come from merging galaxy clusters [11] and the ellipticity of galaxies obtained from X-ray observations [19].

- **Cold:** Dark matter is required to be non-relativistic at the time of structure formation. At most, a small component of the dark matter can be warm (semi-relativistic).

A selection of the more prominent dark matter candidates is shown in Fig. 1.3. The key features of a few of these models are discussed below.

WIMPs

The Weakly Interacting Massive Particle (WIMP) is perhaps the most well-known dark matter candidate. WIMPs rose to fame thanks to the so-called "WIMP miracle" [20]. This refers to the fact that particles with weak scale masses and annihilation cross-sections just so happen to have the correct relic abundance of dark matter when produced via the freeze-out mechanism [21]. In this scenario, the final WIMP abundance depends on the total annihilation cross-section, $\langle \sigma v \rangle$, with only a very mild dependence on the DM mass [22],

$$\Omega_{\mathrm{DM}}h^2 \sim 0.12 \ \left(\frac{2.2 \times 10^{-26}\,\mathrm{cm^3\,s^{-1}}}{\langle \sigma v \rangle} \right). \tag{1.9}$$

The canonical weak-scale WIMP has been tightly constrained from direct and indirect detection limits, leading it to be disfavoured as a dark matter candidate. The term "WIMP" is now typically used to refer to any particle dark matter candidate that is produced thermally in the early Universe. Such a particle can have a mass in the range $10\,\mathrm{MeV} \lesssim m_{\mathrm{WIMP}} \gtrsim 100\,\mathrm{TeV}$. Lighter WIMPs will have non-negligible contributions to the effective number of neutrino species, N_{eff}, which is constrained through BBN and the Cosmic Microwave Background CMB to be $N_{eff} = 2.99 \pm 0.17$ [12]. Masses larger than $\sim 100\,\mathrm{TeV}$ are excluded from partial wave unitarity [23].

Axions

The original axion was proposed by Peccei and Quinn [24] as part of a dynamical solution to the "Strong CP Problem". This refers to the measured value of the neutron electric dipole moment (nEDM) being anomalously small, with a current upper bound of $|d_n| < 0.18 \times 10^{-26}\ e\,\mathrm{cm}$ [25]. This can be translated to an upper bound on the CP-violating QCD θ-parameter such that $|\theta_{QCD}| \lesssim 10^{-10}$, raising questions as to why this value seems to be fine-tuned to such a small value.

The Peccei-Quinn solution to this problem introduces a new, anomalous, global $U(1)_{\mathrm{PQ}}$ symmetry and promotes θ_{QCD} to be a dynamical field. The axion emerges as the pseudo-Goldstone boson associated with the breaking of $U(1)_{\mathrm{PQ}}$, such is in the two most prominent UV completions of the axion, the KSVZ [26, 27] and DFSZ [28, 29] models. In these models, the axion produced in the early Universe can serve the role of cold dark matter today. This makes it a very compelling dark matter candidate, as it solves two of the biggest mysteries of physics in one neat package.

However, solving the Strong CP problem can be rather restrictive on the model parameters. For example, the QCD axion's coupling to the photon is not a free parameter and depends on the scale at which the PQ symmetry is broken. Many

models introduce a light pseudoscalar particle that is not associated with a solution to the Strong CP problem but has a coupling to the photon that takes the same form as the QCD axion. Such pseudoscalars are known as "Axion Like Particles" (ALPs) and can similarly make a good dark matter candidate.

Add some more candidates

1.2.1   Dark Matter in an Effective Fields Theory Framework

1.2.2   Overview of Effective Field Theory

Given the sheer quantity of potential dark matter models and candidates, a model-independent approach for analysing experimental results is often desired. An economic analysis method is to use an Effective Field Theory (EFT) to describe the dark matter-Standard Model interactions. Effective theories are prevalent in all of physics, e.g., describing light using ray optics vs Maxwell's equations or the orbits of planets using Newtonian gravity vs General relativity. The delineating factor in choosing a formalism is the scale (energy, length, etc.) we are interested in. **Add in the usual EFT diagram** Experiments will only be sensitive to interactions that can occur below some energy scale, i.e. $13.6\,\text{TeV}$ at the LHC or $1\,\text{GeV}$ in direct detection experiments; we are only interested in describing the interactions that occur below this scale.

One follows two main schools of thought when constructing an EFT. First, there is the *top-down* approach. Here, you begin with a particular complete model in mind that consists of heavy and light fields. At energies below the production threshold of the heavy fields, these degrees of freedom can be "integrated out" of the theory. This process leaves an effective theory for the interactions amongst the light fields. The interactions that would be mediated by the heavy fields appear as non-renormalisable operators that are suppressed by this high energy scale, Λ.

The second method, known as the *bottom-up* approach, is more agnostic to the high-energy physics that might be in play. In this method, one constructs all possible operators that obey the required symmetries of the theory up to a desired mass dimension. Operators of mass dimension greater than four are then suppressed by powers the required number of powers of the high energy cutoff scale, Λ. This cutoff scale indicates the energy at which the EFT begins to break down and should at least be larger than the masses of the fields in the EFT. The Lagrangian constructed in this manner is made out of a tower of operators, $\mathcal{O}_i^{(n)}$,

forming

$$\mathcal{L}_{\text{EFT}} \supset \sum_{n>4} \sum_{i=1}^{j_n} \frac{C_i^{(n)}}{\Lambda^{n-4}} \mathcal{O}_i^{(n)}, \tag{1.10}$$

where we sum over all j_n operators present at mass dimension n. The $C_i^{(n)}$ are called Wilson coefficients and are typically energy dependent.

In the context of dark matter, there are many EFTs describing the interaction at various energy scales. For example, dark matter scatting off nuclei in direct detection experiments is described by a non-relativistic EFT built out of the momentum transfer, relative velocity and spin operators of the dark matter and targets [30, 31]. At higher energy scales where relativistic effects become important, the EFT is instead constructed from relativistic fields, such as dark matter that may be produced in colliders.

Generally, an EFT will have fewer free parameters than the underlying UV theories, typically the dark matter mass and the high energy cutoff scale. This is in contrast with the dozens or so parameters often present in complete models. This allows for a simpler interpretation of experimental results as you will be fitting to a lower dimensional parameter space.

Move the next sections later?

1.2.3   Dimension 6 EFT Operators for Dirac Fermion Dark Matter

This work's approach will focus on dimension 6 EFT operators that describe the interactions of Dirac fermion dark matter with standard model fermions. These operators will have a structure

$$\mathcal{L}_{\text{EFT}}^{(6)} \sim \frac{1}{\Lambda^2} (\bar{\chi} \Gamma_{\text{DM}} \chi)(\bar{f} \Gamma_{\text{SM}} f), \tag{1.11}$$

where the Γ_i determines the Lorentz structure of the interaction by taking appropriate combinations from the set

$$\Gamma_i \in \{1, i\gamma_5, \gamma^\mu, i\gamma^\mu\gamma^5, \sigma^{\mu\nu}, i\sigma^{\mu\nu}\gamma^5\}. \tag{1.12}$$

For example, the case of $\Gamma_\chi = \Gamma_{\text{SM}} = 1$ yields scalar currents for both the DM and SM fermions and would correspond to integrating out a heavy scalar mediator in the UV theory. There are 10 such operators at dimension six that form a linearly independent basis. These are given in Table 1.1, along with spin-averaged squared matrix element for dark matter scattering with a fermion. The coupling constants,

Name	Operator	g_f	$\lvert\overline{M}(s,t,m_i)\rvert^2$
D1	$\bar\chi\chi\,\bar f f$	$\dfrac{y_f}{\Lambda_f^2}$	$g_f^2\dfrac{\left(4m_\chi^2-t\right)\left(4m_\chi^2-\mu^2 t\right)}{\mu^2}$
D2	$\bar\chi\gamma^5\chi\,\bar f f$	$i\dfrac{y_f}{\Lambda_f^2}$	$g_f^2\dfrac{t\left(\mu^2 t-4m_\chi^2\right)}{\mu^2}$
D3	$\bar\chi\chi\,\bar f\gamma^5 f$	$i\dfrac{y_f}{\Lambda_f^2}$	$g_f^2 t\left(t-4m_\chi^2\right)$
D4	$\bar\chi\gamma^5\chi\,\bar f\gamma^5 f$	$\dfrac{y_f}{\Lambda_f^2}$	$g_f^2 t^2$
D5	$\bar\chi\gamma_\mu\chi\,\bar f\gamma^\mu f$	$\dfrac{1}{\Lambda_f^2}$	$2g_f^2\dfrac{2\left(\mu^2+1\right)^2 m_\chi^4-4\left(\mu^2+1\right)\mu^2 s m_\chi^2+\mu^4\left(2s^2+2st+t^2\right)}{\mu^4}$
D6	$\bar\chi\gamma_\mu\gamma^5\chi\,\bar f\gamma^\mu f$	$\dfrac{1}{\Lambda_f^2}$	$2g_f^2\dfrac{2\left(\mu^2-1\right)^2 m_\chi^4-4\mu^2 m_\chi^2\left(\mu^2 s+s+\mu^2 t\right)+\mu^4\left(2s^2+2st+t^2\right)}{\mu^4}$
D7	$\bar\chi\gamma_\mu\chi\,\bar f\gamma^\mu\gamma^5 f$	$\dfrac{1}{\Lambda_f^2}$	$2g_f^2\dfrac{2\left(\mu^2-1\right)^2 m_\chi^4-4\mu^2 m_\chi^2\left(\mu^2 s+s+t\right)+\mu^4\left(2s^2+2st+t^2\right)}{\mu^4}$
D8	$\bar\chi\gamma_\mu\gamma^5\chi\,\bar f\gamma^\mu\gamma^5 f$	$\dfrac{1}{\Lambda_f^2}$	$2g_f^2\dfrac{2\left(\mu^4+10\mu^2+1\right)m_\chi^4-4\left(\mu^2+1\right)\mu^2 m_\chi^2(s+t)+\mu^4\left(2s^2+2st+t^2\right)}{\mu^4}$
D9	$\bar\chi\sigma_{\mu\nu}\chi\,\bar f\sigma^{\mu\nu} f$	$\dfrac{1}{\Lambda_f^2}$	$8g_f^2\dfrac{4\left(\mu^4+4\mu^2+1\right)m_\chi^4-2\left(\mu^2+1\right)\mu^2 m_\chi^2(4s+t)+\mu^4(2s+t)^2}{\mu^4}$
D10	$\bar\chi\sigma_{\mu\nu}\gamma^5\chi\,\bar f\sigma^{\mu\nu} f$	$\dfrac{i}{\Lambda_f^2}$	$8g_f^2\dfrac{4\left(\mu^2-1\right)^2 m_\chi^4-2\left(\mu^2+1\right)\mu^2 m_\chi^2(4s+t)+\mu^4(2s+t)^2}{\mu^4}$

Table 1.1: Dimension 6 EFT operators [32] for the coupling of Dirac DM to fermions (column 2), together with the squared matrix elements DM-fermion scattering (column 5), where s and t are Mandelstam variables, $\mu = m_\chi/m_T$, and m_T is the target mass.

g_f, are given in terms of the fermion Yukawa couplings, y_f, and the EFT cutoff scale, Λ_f. Hence, these operators describe interactions between dark matter and the elementary fermions of the Standard Model: the leptons and quarks.

1.2.4 Going from DM-Quark to DM-Nucleon Interactions

The operators in Table 1.1 describe dark matter interactions at the quark level, as these are the degrees of freedom most models are formulated with. However, we will primarily be interested in dark matter scattering with baryons, which requires taking the matrix element of the quark operators between baryon states, i.e. $\langle\mathcal{B}|\bar q\,\Gamma_q q|\mathcal{B}\rangle$. These matrix elements can be calculated through the application of Chiral Perturbation Theory (ChPT), giving a baryon level EFT. The operators of this EFT will have the same form as those in Table 1.1, with the obvious replacement of $f \to \mathcal{B}$, as well as additional form factors that take into account the structure of the baryons.

The required form factors for each operator have been calculated at zero mo-

mentum transfer in Ref. [30] and are given by

$$c_{\mathcal{B}}^{S}(0) = \frac{2m_{\mathcal{B}}^2}{v^2} \left[\sum_{q=u,d,s} f_{T_q}^{(\mathcal{B})} + \frac{2}{9} f_{T_G}^{(\mathcal{B})} \right]^2, \tag{1.13}$$

$$c_{\mathcal{B}}^{P}(0) = \frac{2m_{\mathcal{B}}^2}{v^2} \left[\sum_{q=u,d,s} \left(1 - 3\frac{\overline{m}}{m_q}\right) \Delta_q^{(\mathcal{B})} \right]^2, \tag{1.14}$$

$$c_{\mathcal{B}}^{V}(0) = 9, \tag{1.15}$$

$$c_{\mathcal{B}}^{A}(0) = \left[\sum_{q=u,d,s} \Delta_q^{(\mathcal{B})} \right]^2, \tag{1.16}$$

$$c_{\mathcal{B}}^{T}(0) = \left[\sum_{q=u,d,s} \delta_q^{(\mathcal{B})} \right]^2, \tag{1.17}$$

where $v = 246$ GeV is the vacuum expectation value of the SM Higgs field, $\mathcal{B}$ is the baryonic species, $\overline{m} \equiv (1/m_u + 1/m_d + 1/m_s)^{-1}$ and $f_{T_q}^{(\mathcal{B})}$, $f_{T_G}^{(\mathcal{B})} = 1 - \sum_{q=u,d,s} f_{T_q}^{(\mathcal{B})}$, $\Delta_q^{(\mathcal{B})}$ and $\delta_q^{(\mathcal{B})}$ are the hadronic matrix elements, determined either experimentally or by lattice QCD simulations[1]. The specific values of these matrix elements for various baryons are provided in Appendix **ADD APPENDIX**.

These form factors are perfectly viable when considering interactions with momentum transfers $\lesssim 1\,\mathrm{GeV}$ such as in direct detection experiments. For energies greater than this, the internal structure of the baryon begins to be resolved, and an additional momentum-dependent form factor is required to account for this [33],

$$F_{\mathcal{B}}(t) = \frac{1}{(1 - t/Q_0)^2}, \tag{1.18}$$

where t is the Mandelstam variable, and Q_0 is an energy scale that depends on the hadronic form factor. For simplicity, we will conservatively take $Q_0 = 1\,\mathrm{GeV}$ for all operators. Putting everything together, the squared coupling constants for dark matter-baryon interactions are obtained by making the replacement

$$g_f^2 \to \frac{c_{\mathcal{B}}^I(t)}{\Lambda_q^4} \equiv \frac{1}{\Lambda_q^4} c_{\mathcal{B}}^I(0) F_{\mathcal{B}}^2(t), \quad I \in S, P, V, A, T, \tag{1.19}$$

in the matrix elements in the final column of Table 1.1.

---

[1]The superscript letters S, P, V, A and T stand for Scalar, Pseudoscalar, Vector, Axial-vector and Tensor interactions respectively. The corresponding operators are: D1-2 for S; D3-4 for P; D5-6 for V, D7-8 for A; and D9-10 for T.

1.3 Current Status of Dark Matter Constraints

In broad terms, there are three main ways that we can search for evidence of dark matter, often termed "make it, shake it or break it". "Make it" refers to dark matter being produced at colliders; "break it" to searching for dark matter annihilation signals; and "shake it" to direct detection of dark matter scattering. An illustrative way of depicting these processes is shown in Fig. **add usual diagram**. This section discusses the current status of these detection methods.

1.3.1 Collider Bounds

If dark matter is produced in a collider, it will simply leave the detector without depositing any energy. In order to determine if such an invisible particle was produced, conservation of energy-momentum is used to determine if there are any events that are missing energy. In practice, what is searched for is missing momentum that is transverse to the beamline.

Currently, dark matter has not been observed to be produced in particle colliders. This non-observation has instead been used to constrain the dark matter mass and production cross sections or couplings of various models. These limits are typically interpreted in a model-dependent manner, as different dark matter - Standard model couplings can significantly alter the production rates. As mentioned above, EFTs can be used to explore a variety of interactions in a somewhat model-independent way. However, many applications of this nature did not hold up to scrutiny, as the EFTs were being applied at energies outside their regions of validity [34–37], and so care is needed when applying such methods.

The ATLAS and CMS experiments at the LHC have performed analyses on various dark matter production mechanisms, including the exchange of a Z/Z' or Higgs, EFTs and heavy mediators, and mono-jet searches [38] [2]. Collider searches also offer complimentary probes of the dark matter-nucleon scattering cross-section [39].

It is important to note that an observation of an invisible massive particle at a collider is not enough to infer that it is dark matter. Such an observation only tells us that such a particle exists but nothing about its abundance, meaning it could just be a sub-component of a larger dark sector. In order to identify whether or not this was a dark matter detection, complimentary observations from direct or indirect detectors would be required.

---

[2]These searches refer to a single jet being produced alongside a pair of dark matter particles. This jet could be of Standard Model or dark sector origin, with the latter commonly referred to as "mono-X" searches.

1.3.2 Direct Detection Searches

Direct detection experiments vary wildly depending on the dark matter mass range they are trying to probe. For ALP dark matter that is wavelike, haloscope experiments such as ADMX [40] and MADMAX [41] attempt to convert ALPs to photons via the Primakoff effect. Searches for WIMP dark matter look for the dark matter scattering with some detector material, causing it to recoil and release some energy. Given our focus on WIMP dark matter, this section will review the experimental status of these detectors.

The differential rate at which the incoming flux of dark matter will scatter within a detector with N_T targets, as a function of the recoil energy, E_R, is given by

$$\frac{dR(E_R, t)}{dE_R} = N_T \frac{\rho_{\text{DM}}}{m_{\text{DM}}} \int_{v > v_{\text{min}}}^{v_{\text{esc}}} v f(\vec{v} + \vec{v}_E) \frac{d\sigma}{dE_R} d^3 v, \tag{1.20}$$

and depends on the quantities:

- v_{min} is the minimum dark matter velocity required by kinematics for a scattering event to occur;

- $v_{\text{esc}} = 528 \, \text{km s}^{-1}$ is the Milky Way escape velocity;

- $\vec{v}_E$ is the velocity of the Earth through the dark matter halo[3];

- $f(\vec{v} - \vec{v}_E)$ is the dark matter velocity distribution in the Earth's frame;

- $d\sigma/dE_R$ is the differential scattering cross-section.

Given the low interaction rate of dark matter, the expected event rate in detectors is very low, around one event per day, per kilogram of target material, per kiloelectronvolt deposited. Having such a low event rate requires the detector to be situated in an extremely low background environment, such as underground laboratories.

Direct detection experiments aim to probe two main types of dark matter interactions: Spin-dependent (SD) and spin-independent (SI) scattering. SD interactions couple to the overall spin of the target, while SI interactions are agnostic to this. Therefore, experiments searching for SI interactions benefit from using nuclei with a large atomic number, A, as the interaction cross-section will involve a coherent sum over all nucleons. This leads to an A^2 enhancement of SI interactions compared to the SD counterpart.

---

[3]This accounts for the orbit of the Earth around the Sun, which induces an annual modulation in the flux of DM.
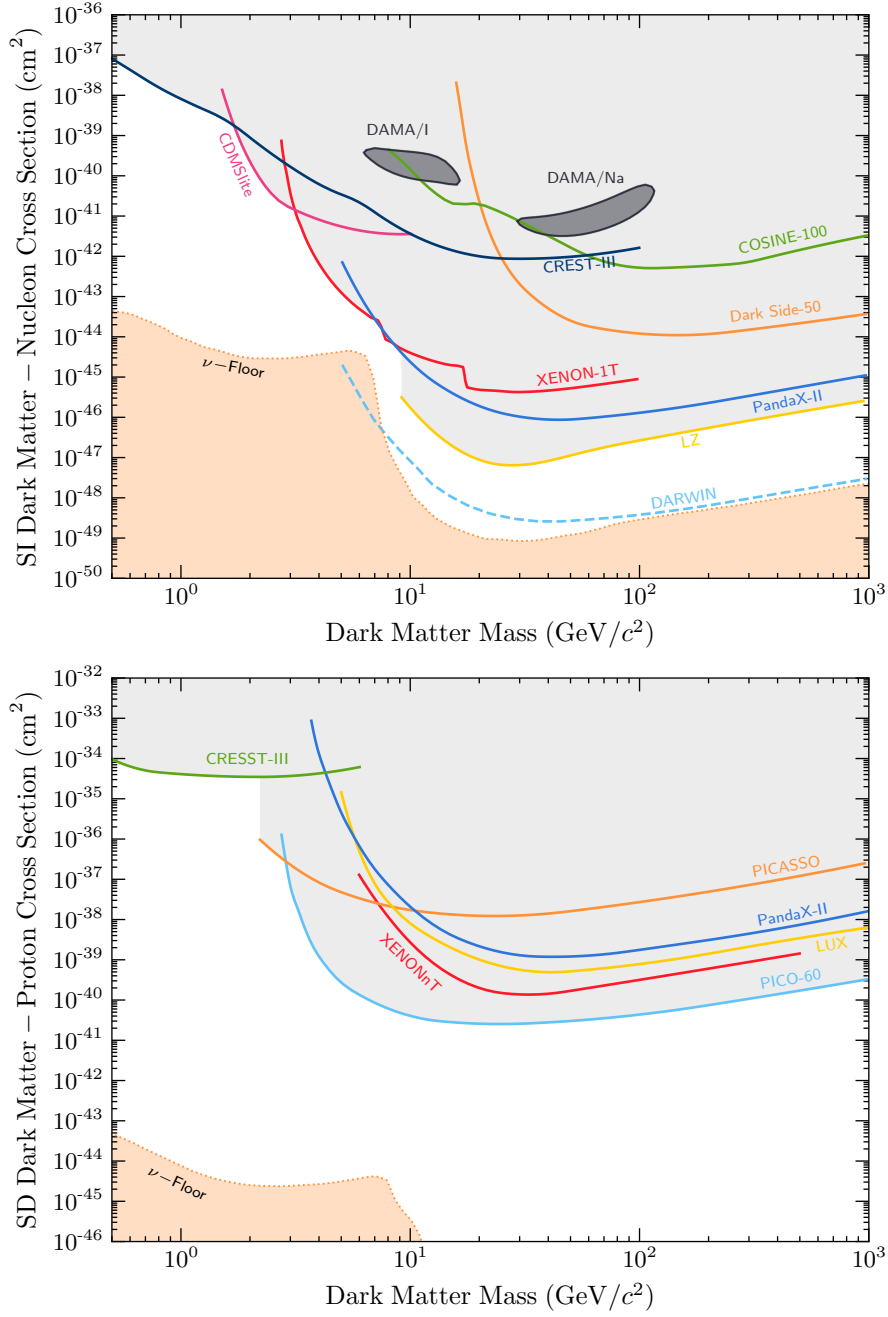
Figure 1.4: Current status of direct detection searches for dark matter. **Top:** Spin-independent dark matter-nucleon scattering. **Bottom:** Spin-dependent dark matter-proton scattering.

The current leading constraints on the dark matter-nucleon scattering cross-section are shown in Fig. 1.4, with SI in the top panel and SD in the bottom. The SI limits are set by liquid noble gas experiments (LZ [42], XENON-1T [43], PandaX-II [44], and DarkSide-50 [45]), solid-state cryogenic detectors (CRESST-III [46], CDMSlite [47], with projected DARWIN sensitivities [48]), and room temperature crystals (DAMA/LIBRA [49], and COSINE-100 [50]).

The SD experiments require their targets to carry non-zero spin for the dark matter to couple to. ^{19}F is the favourable choice proton scattering, as it has an unpaired proton giving it its overall spin. The leading constraints come from superheated liquid experiments such as the PICO-60 [51] as well as PICASSO [52] In terms of the SD proton scattering shown in Fig 1.4, These interactions are also searched for by many of the same experiments in the SI case, with the inclusion of LZ's predecessor LUX [53].

The orange dashed line represents the neutrino floor[4], a theoretical lower limit on the discoverability of WIMP-like dark matter. In this region of parameter space, doctors will become sensitive to the irreducible background from neutrino scattering, which will produce signals almost indistinguishable from a true dark matter interaction. A significant amount of effort is being put toward overcoming this hindrance, with the main strategy being to take advantage of the directionality of dark matter flux [55].

Many experiments begin to lose sensitivity to low-mass dark matter ($m_{\mathrm{DM}} \lesssim 10\,\mathrm{GeV}$) as the targets recoil with energies below the detector threshold. Current energy thresholds can reach as low as $\sim \mathcal{O}(100\,\mathrm{eV})$, which is on the same order of magnitude as the recoil energy due to a 1 GeV dark matter collision. The sensitivity also falls off at a slower rate at larger masses, though this is due to the number of dark matter particles that pass through the detector given $N_{\mathrm{DM}} = \rho_{\mathrm{DM}}/m_{\mathrm{DM}}$, and the dark matter density is known to be $0.4\,\mathrm{GeV\,cm^{-3}}$.

Direct detection limits also assume that the scattering cross-section is independent of the dark matter velocity and momentum transfer in the interaction. Given that the local dark matter dispersion velocity is predicted to be $v_d = 270\,\mathrm{km\,s^{-1}} \approx 10^{-3}c$, a back-of-the-envelope estimation for the momentum transfer gives $q_{\mathrm{tr}} \lesssim 100\,\mathrm{MeV}$. Therefore, cross-sections proportional to v_{DM} or q_{tr} will result in significantly lower event rates and hence much weaker limits than the unsuppressed interactions.

This leads us to indirect detection methods, which can provide complementary probes to direct detection while also exploring interactions that are difficult, if not impossible, for terrestrial-based detectors to observe.

---

[4]Calling this the "neutrino fog" rather than floor has been gaining traction in recent years [54]

1.3.3 Indirect Detection

Indirect detection experiments aim to infer the presence of dark matter through its annihilation or decay into Standard Model states. These searches look for anomalies in astrophysical data, though dark matter accumulating within the Earth's core can also produce a detectable signal [56, 57]. The signals searched for include:

- Gamma-rays at terrestrial-based telescopes such as HESS [58–60], VERI-TAS [61–63], MAGIC [64, 65] and HAWC [66–69] as well as the Fermi-LAT [70–74] satellite;

- Neutrino signals at IceCube [75, 76], ANTARES [57, 77, 78], Super-K [79–81], and will be searched for at the upcoming Hyper-K [82–84], JUNO [85] experiments.

- Cosmic-Rays by the AMS-02 experiment [86, 87]

Signals from dark matter annihilation are best searched for by looking at regions where the dark matter density is expected to be high, boosting the annihilation rate. Natural places to look include the Galactic Centre [88, 89], dwarf-spheroidal galaxies [90], and celestial bodies where dark matter can accumulate over time. This last option is of primary interest to this work.

Stars have long been used to study various models of dark matter. ALPs of dark photons can be produced within the plasma of stars, altering the energy transport properties within them. This can ultimately lead to deviations in the evolution of the star, which can be used to place some of the strongest constraints on these models [91–93]. WIMP-like dark matter from the halo that couples to visible matter can scatter within the objects. The dark matter may lose enough energy in these interactions to become gravitationally bound to the object, leading to a population of dark matter being accumulated over time [21, 94–97].

The capture of dark matter within the Sun has been extensively studied. The formalism set up by Gould [95, 96, 98] has remained quite successful, with many authors building on these foundations over time [97, 99, 100] The captured dark matter can thermalise within the Sun's core, where it may annihilate and produce an observational signal. This could be via direct annihilation to neutrinos [77–79, 101, 102], or to some other long-lived state that can escape the Sun and decay into visible states [103–107]. Additionally, WIMPs can also alter the energy transport within the Sun [108–111].

In comparison to DD searches, interpretation of indirect detection data will require additional model-dependent assumptions, namely the relevant annihilation channels of the dark matter. The most general limits can be placed by assuming that the dark matter only has a single annihilation channel, i.e. it annihilates to a $\tau^+\tau^-$ final state 100% of the time. Under these assumptions, limits on the SD dark
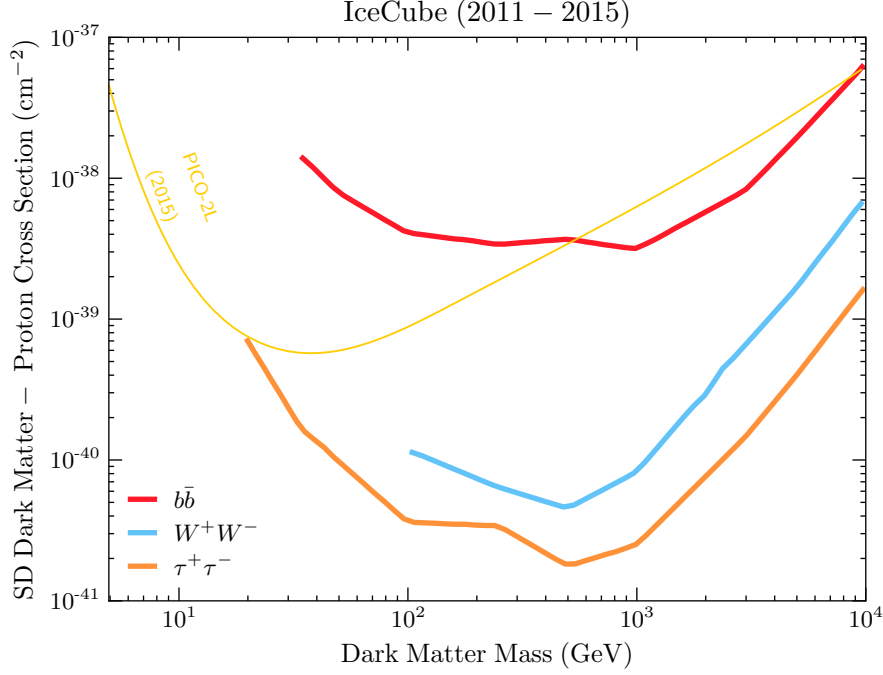
Figure 1.5: Limits on the SD dark matter-proton cross-section from the IceCube collaboration assuming 100% branching fraction to $b\bar{b}$ (red), W^+W^- (blue) or $\tau^+\tau^-$ (orange) final states. Also shown is the result from the PICO-2L DD experiment. This plot was recreated with data taken from Ref. [75].

matter-proton cross-section have been placed that exceed current DD constraints, due to the rather large abundance of Hydrogen within the Sun. Constraints from the IceCube collaboration are shown in Fig. 1.5

The smallest dark matter mass that can be probed using solar capture is determined by the evaporation mass of the Sun. Below this mass, the dark matter will be efficiently evaporated out of the Sun at the same rate it is captured, thus no annihilation can take place [5]. Additionally, as with direct detection, the Sun will be far less sensitive to interactions that are proportional to the velocity/momentum transfer.

Overcoming the first issue requires either a colder star or one that is much heavier. The second requires dark matter to scatter with the constituent material at relativistic energies to overcome the suppression in the cross-sections. Fortunately, there exists objects that meet all these criteria, allowing for a wider variety of dark matter models to be explored then direct detection or traditional indirect detection experiments: compact objects.

---

[5]A more rigorous definition of evaporation and evaporation mass will be presented later in the thesis.

1.4   Compact Objects as Dark Matter Probes

The main goal behind this work is to explore how compact objects can be used to probe a wide variety of dark matter interactions that terrestrial direct detection experiments are insensitive to. By compact objects, we are referring to Neutron Stars (NSs) and White Dwarfs (WDs), and not Black Holes that also fall into this category.

Compact objects offer a unique laboratory for studying dark matter and its interactions with the Standard Model in environments unachievable anywhere else in the Universe. They generate strong gravitational fields and are composed of incredibly dense matter, with NSs reaching super-nuclear densities in their central cores. The capture rate within these objects is therefore enhanced due to these properties, with benefits over solar capture including:

- **Gravitational focusing of the DM flux:** The strong gravitational field will increase the impact parameter of the infalling dark matter. This increases the effective size of the capturing body, increasing the flux of dark matter passing through it.

- **Realtivistic Interaction Energies:** In general, the infalling dark matter will be accelerated to (semi-)relativistic velocities ($\sim 0.2 - 0.7c$). Moreover, the stellar constituents will also have relativistic energies. As such, interactions that are momentum/velocity dependent will suffer far less suppression than in DD experiments.

- **Large Number of Targets:** The extremely high densities of these objects correspond to a considerable number of targets for scattering to occur. This allows these objects to probe very small scattering cross-sections, with NSs in particular expected to reach as low as $\sim 10^{-45}\,\mathrm{cm}^2$.

- Forgot the last point....

In the past, capture in NSs has been applied primarily in the context of sending gravitational collapse into black holes [112–118], and the modifications of NS merger rates as well as the gravitational wave signatures of these mergers [119–122]. Capture in WDs has also been considered, with a variety of different applications of the capture process [123–128].

In recent years, dark matter induced heating of NSs has reemerged as a potential detection frontier [129–136]. It was shown that dark matter could reheat old, isolated NSs in our local neighbourhood back up to temperatures that would cause them to radiate as blackbody peaked in the near-infrared. The aim is to locate the NSs with radio telescopes such as the Square-Kilometer-Array (SKA), and determine their age through their spindown rate. Once located, the star's temperature
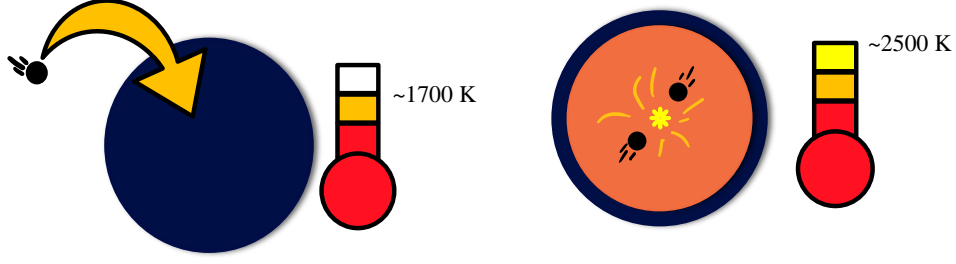
Figure 1.6: Illustration of DM-induced heating of compact objects. **Left:** kinetic heating due to DM scattering, raising the temperature to $\sim 1700\,\text{K}$. **Right:** Annihilation heating contributes an additional $\sim 800\,\text{K}$. This image is inspired by Ref. [129].

can be determined through observations from infrared telescopes such as the James Webb Space Telescope (JWST).

This heating occurs in two stages. The dark matter will first deposit its kinetic energy into the star through the scatterings required for capture and its subsequent thermalisation within the NS core, with this process called *kinetic heating*. If the dark matter can annihilate, it will deposit its mass energy, assuming the products are trapped within the star, termed *annihilation heating*. These processes are illustrated in Fig. 1.6. Assuimng a NS in our local neighbourhood, i.e., within

In order to accurately determine the limits on dark matter interactions that such an observation could place, one first requires an accurate calculation of the capture rate. However, all previous calculations relied on the formalism set up by Gould for capture in the Sun, with only minor modifications made to accommodate the extreme nature of the compact objects.

Chapters **??** and **??** of this thesis are devoted to reformulating Gould's capture formalism to account for the physics specific to compact objects in a self-consistent manner. These include a relativistic treatment of the kinematics, using General Relativity to calculate the correct dark matter flux passing through the star, and accounting for Pauli blocking of the final state target using Fermi-Dirac statistics for the stellar constituents. In addition, we incorporate the internal structure of these objects by calculating the radial profiles for the relevant microscopic quantities (e.g., chemical potentials and number densities) via the adoption of a realistic equation of state.

Further considerations are required when considering dark matter interactions with the baryonic matter inside NSs. Due to the high density of the NS interior, the baryonic matter undergoes strong interactions amongst themselves and should not be treated as a free Fermi gas. Instead, adopting an equation of state that accounts for these interactions is required. These interactions modify the mass of the baryons, leading them to obtain an effective mass smaller than their vacuum

mass. Furthermore, as we will see, the dark matter may interact with the baryons with momentum transfers on the order of $10\,\mathrm{GeV}$. This is high enough that the dark matter will begin to resolve the internal structure of the baryon. To account for this, the momentum dependence of the baryon form factors that are typically neglected in direct detection and solar capture must be reintroduced.

This formalism is made in preparation for a thorough analysis of the timescales involved in the dark matter heating of compact objects. The enrgy deposited in both the kinetic and annihilation heating stages does not occur instantaneously, and the timescales involved in them need to be compared to the age of the star in question. We will define kinetic heating timescale as the time required for dark matter to deposit 99% of its initial kinetic energy into the star. For annihilation heating to occur, the dark matter must reach a state of capture-annihilation equilibrium within the stellar core. In standard calculations of this timescale, the dark matter must first become thermalised with the star. Only then can annihilations occur efficiently enough to heat the star.

We will work with the EFT operators in Table 1.1 that describe Dirac fermion dark matter interacting with Standard Model leptons. Each operator will be studied in isolation, i.e., by considering a Lagrangian that contains only one of the operators rather than a linear superposition of multiple. This way, we can analyse specific types of interactions independently, allowing us to take as model-independent an approach to phenomenology as possible.